1990

Calculated thermodynamic properties and phase transitions of solid N2 at temperatures 0≤T≤300 K and pressures 0≤P≤100 GPa

J. Belak, *Johns Hopkins University*
Richard Alan Lesar, *Los Alamos National Laboratory*
R. D. Etters, *Colorado State University*

Calculated thermodynamic properties and phase transitions of solid N2 at temperatures 0T300 K and pressures 0P100 GPa

J. Belak, R. LeSar, and R. D. Etters

Citation: The Journal of Chemical Physics **92**, 5430 (1990); doi: 10.1063/1.458521
View online: http://dx.doi.org/10.1063/1.458521
View Table of Contents: http://scitation.aip.org/content/aip/journal/jcp/92/9?ver=pdfcov
Published by the AIP Publishing

Calculated thermodynamic properties and phase transitions of solid N_2 at temperatures $0 \leqslant T \leqslant 300$ K and pressures $0 \leqslant P \leqslant 100$ GPa

J. Belak
Department of Physics and Astronomy, Johns Hopkins University, Baltimore, Maryland 21218

R. LeSar
Los Alamos National Laboratory, Los Alamos, New Mexico 87545

R. D. Etters
Department of Physics, Colorado State University, Fort Collins, Colorado 80523

(Received 24 November 1989; accepted 10 January 1990)

Thermodynamic properties of solid nitrogen are calculated over a variety of isotherms and isobars using a constant pressure Monte Carlo method with deformable, periodic boundary conditions. Vibron frequencies are calculated using a simple perturbation theory. In addition, pressure–volume relations, thermal expansion coefficients, structures, and phase transition pressures and temperatures are determined. In particular, the nature of the orientational disorder in the plastic crystal phases is examined by calculating a variety of orientational order parameters.

I. INTRODUCTION

Condensed phases of nitrogen continue to be the object of intensive investigation, partially because N_2 is abundant and a part of many important physical processes, and because the electronic charge distribution of the molecule is unusually stable by virtue of a strong, triple covalent bond. As evident from the phase diagram [Fig. 1] many different structures exist with a wide variety of properties.

The modification of N_2 at the lowest temperatures and pressures is the cubic Pa3 phase[1–3] where the molecules orient along the four cube body diagonals. At normal vapor pressure there is a phase transition into a hexagonal close packed $P6_3/mmc$ structure[2,4] at $T = 35.6$ K, which persists until melting at $T = 63.1$ K. This plastic crystal phase, known as β-N_2, is characterized by its structural order but orientational disorder. Measurements have not unambiguously identified the nature of this disorder.[6–9] An early interpretation[6] was that the molecules freely precess about the c axis at an angle of approximately 56°, although it was recognized that the data could be understood equally well in terms of a model in which all orientations were equally probable. Interpretations of the latter model as a characterization of nearly free rotor behavior or a random static orientational disorder have also been considered.

As the pressure is increased along the 300 K isotherm, fluid N_2 freezes into β-N_2 at $P = 2.44$ GPa,[10,11] which presists to $P = 4.90$ GPa, where a transition into the cubic Pm3n phase occurs.[12] This δ phase has eight molecules per unit cell, with a peculiar orientational disorder. Using Fig. 2 as a guide, scattering measurements indicate that the molecules at the corners and at the center of the cube have a spherically symmetric orientational distribution.[12–16] As for β-N_2, it has not been experimentally established if these molecules act as free rotors or randomly orient along the four body diagonals. An intermediate possibility is that these molecules cooperatively flip from along one body diagonal to another over a time scale long compared to a free rotation period. Then, the average over these four degenerate configurations could also give the observed scattering profile. Along each face of this structure there are two molecules whose centers lie on a line parallel to one of the crystal axes. Experimental evidence is that they exhibit a random orientation in a planar disk normal to the unit cell face, as shown in Fig. 2. As with the spherical site molecules, it is not known if the orientational distribution is a result of nearly free planar rotation, a random but static planar distribution, or periodic, cooperative rearrangements from one degenerate orientation to another.[12–16] Raman scattering measurements[13,15] of the vibron frequencies show two branches[14,17] characteristic of the Pm3n structure until $P \simeq 17.5$ GPa, at which point the lowest branch splits into three or four modes. This signals a change of symmetry associated with a phase transition into a

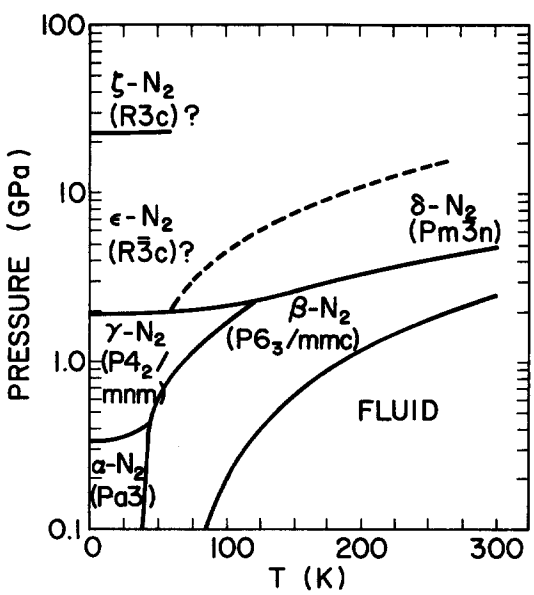

FIG. 1. The phase diagram of N_2.

[a] Present address: Department of Physics, H-Division, Lawrence Livermore National Laboratory, P.O. Box 808, Livermore, California 94550.

 0021-9606/90/095430-12$03.00

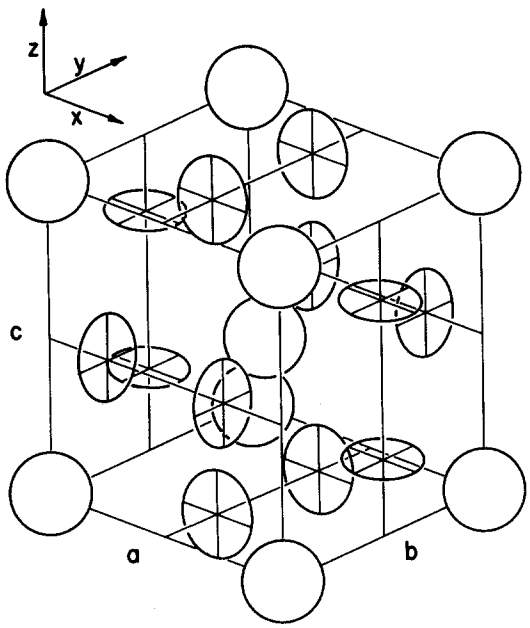

FIG. 2. The cubic Pm3n structure of molecular nitrogen. The open circles on the corner and body centered sites depict a spherically symmetric orientation distribution. The two crossed circles projecting from each face depict a uniform orientational distribution in the plane of the circle (disk).

structure that has not been identified, nor has the nature of the orientational order.

As the temperature is lowered from 300 K along the 7 GPa isobar, x-ray diffraction measurements[18] indicate that the cubic Pm3n phase persists down to approximately 140 K where a transition occurs into a structure without cubic symmetry. A reasonable interpretation of the data is consistent with a rhombohedral $R\bar{3}c$ structure, again with eight molecules per unit cell. In fact, that structure is very similar to Pm3n but with the orientational disorder frozen out, which would be expected to lower the symmetry. However, other possibly more complicated structures have not been ruled out. Theoretical calculations,[19,20] using an eight molecule unit cell, have predicted the stability of the $R\bar{3}c$ structure. This contradicts the original simulation results of Nosé and Klein,[21] who predicted a phase change into a tetrahedral structure at a temperature close to the observed value.[18] The results of this work are, at least qualitatively, in agreement with those predictions.[21] We now believe that the $R\bar{3}c$ results[19,20] were the consequence of an incomplete optimization of the crystal. Thus, theory now seems to be at odds with experiment.

Upon increasing the pressure above 7 GPa along the 15 K isotherm, Raman data[15] shows a splitting of the lower frequency vibron branch at $P \simeq 20$ GPa, which is very similar to that observed at room temperature[17] and higher pressure. The structure is not known, but it has been speculated that it is a lower symmetry R3c variant of the $R\bar{3}c$ structure.

The objective of this work is to examine the properties of solid N_2 along the isobars and isotherms discussed above. A major objective is to provide new understanding of the orientational disorder in the plastic crystal phases and determine the nature of the transitions associated with them. In addition, equations of state, thermal expansion, vibron frequencies, and structural predictions are made over a wide range of temperatures and pressures.

II. METHOD AND POTENTIALS

The total potential energy of the crystal is described by the sum of three expressions,

$$U_T = \sum_{i<j} \sum_{s=1}^{4} U_V[R_{ij}(s)] + U_{\mathrm{EMP}} + U_{\mathrm{intra}}, \qquad (1)$$

where $\Sigma_s U_V[R_{ij}(s)]$ is an atom–atom expression for the van der Waals interaction between a pair of molecules (i,j), and $R_{ij}(s)$ is the distance between atoms on two different molecules. Thus, there are four different values for R between two diatomic molecules. This expression was formed from our fit[22] to *ab initio* results[23] at intermediate and long range and to electron gas calculations[24] at short range. The electric multipole interactions U_{EMP} are formed by placing four point charges along each molecular axis, and summing the Coulomb interaction between charges on different molecules.[23] The intramolecular interactions are represented by an extended Rydberg expression.[25] U_{intra} also contains a simple classical expression for the energy of a free rotor, which depends on the molecular bond length and the temperature. Details of the total potential have been presented elsewhere.[22,26,27]

Averages of thermodynamic quantities were determined using a constant pressure Monte Carlo method with deformable, periodic boundary conditions. The number of molecules in the Monte Carlo cell ranged from 64 to 512, depending on thermodynamic conditions. These, and a few runs with 32 molecules in the fluid state, were sufficient to show the absence of any significant size effects. Lattice sums were typically taken out to 9 Å, with continuum corrections beyond that, and at least 5000 steps were run at each (N,P,T) point to obtain averages after initial transients were eliminated. Each step consists of a separate random move of the position and orientation of each molecule and the coordinates of the Monte Carlo cell. The probability $P(X)$, of any physical quantity, is determined from the instantaneous values of X along the Monte Carlo trajectory, binned in small subintervals ΔX. The distribution of expectation values $D(\langle X \rangle)$ is determined by first evaluating all possible independent estimates of $\langle X \rangle$, then binning the resulting values. Errors are estimated from subaverages $\langle X \rangle_{\mathrm{Bin}}$, evaluated within bins of 100 Monte Carlo steps. For further details, the reader is referred to Ref. 26.

The pressure–temperature dependence of the intramolecular vibron mode frequencies were calculated using a simple perturbation theory.[27] All Monte Carlo runs were performed using the gas phase equilibrium bond length $r_e = 1.097\,68$ Å, and the average force along each molecular axis, $\langle \partial U_T/\partial r_i \rangle$; $i = 1,...,N$, was calculated at every P,T point. Here r_i is the instantaneous bond length of the ith molecule. The equilibrium bond length was then changed until the force on each atom is zero, giving an equilibrium value $r_m(P,T)$, and the derivatives

$$(\partial^s U_T/\partial r^s)_{r_m} = k_s, \quad s = 2,3,4$$

were evaluated for each molecule to give the quadratic, cubic, and quartic force constants. Then standard perturbation theory was applied to determine the vibron frequencies for each molecule,

$$\nu(P,T) = (k_2/\mu)^{1/2} + \frac{3\hbar}{\mu k_2}[k_4 - 5(k_3)^2/2k_2], \quad (2)$$

where μ is the reduced mass of the molecule.

III. RESULTS

The description of the phases along certain isotherms and isobars, given in Sec. I, was designed to compliment the calculations that were made along these same paths. Following is a synopsis of the results which include various thermodynamic quantities, pressure and temperature dependence of the vibron frequencies, details of the orientational disorder, and an analysis of the transitions.

A. β-N_2 at zero external pressure

Over the range $35.6 \leqslant T \leqslant 63.1$ K, the experimentally observed[2-5] hexagonal close packed structure was also found to be stable by calculation, and the c/a ratio at all temperatures is within the statistical uncertainty ($\pm 0.7\%$) of its ideal value, which is in agreement with experiment. The solid line in Fig. 3 shows the calculated molar volume versus temperature of β-N_2, and the circle[28] and squares[29] represent experimental data. The statistical uncertainty in the calculated curve is ± 0.004 cm^3/mol at each temperature. The solid line in Fig. 4 shows the experimentally measured[29] volume thermal expansion coefficient β versus temperature, and the solid squares are calculated values. Although the numerical agreement with experiment is not everywhere excellent, the qualitative features do agree. That is, β, not to be confused with the phase, initially decreases with increasing temperature and then rises sharply near the melting point. Three other points have been calculated in the β phase at a pressure $P = 0.4$ GPa. They are (P,V,T) equals (0.4 GPa, 25.82 cm^3/mol, 100 K), (0.4 GPa, 25.30 cm^3/mol, 75 K), and (0.4 GPa, 24.93 cm^3/mol, 55 K). Our calculated volume at this latter point is to be compared with a measured value[7] of 24.34 ± 0.012 cm^3/mol.

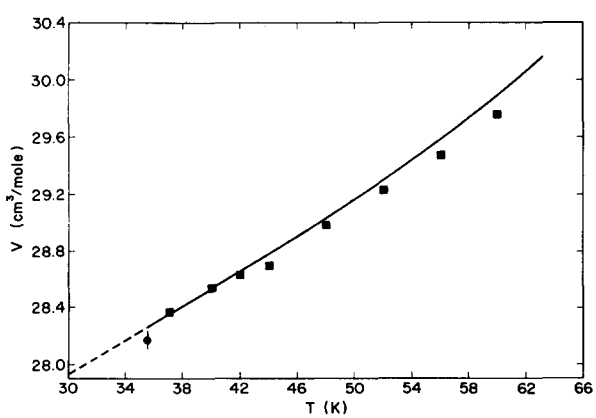

FIG. 3. The solid squares and circle represent experimentally measured volumes (Refs. 28 and 29) in the β phase versus temperature, at zero external pressure. The solid line represents the calculated values.

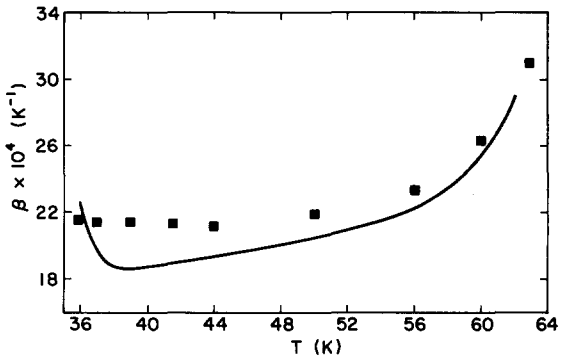

FIG. 4. The solid line represents the measured thermal expansion coefficient in the β phase versus temperature and the solid squares represent calculated values. The statistical error is of the order of the symbol size.

Although we have examined the orientational characteristics of β-N_2 over a range of temperatures, we focus here on the point $T = 55$ K, $P = 0.4$ GPa, because it has been the subject of extensive neutron scattering studies.[7] The solid line on Fig. 5 shows the distribution function $D(\langle \hat{n}_i \cdot \hat{n}_j \rangle)$, calculated over all pairs of molecules (i,j) in the Monte Carlo cell, where $\hat{n}_i$ is the unit vector identifying the direction of the molecular axis of molecule i. Thus, $\hat{n}_i \cdot \hat{n}_j$ equals $\cos\theta_{ij}$, the angle between molecular axes of (i,j). Similarly, the dashed line give the distribution of $\langle (\hat{n}_i \cdot \hat{n}_j)^2 \rangle$. Note that the mean value of these quantities are zero and 0.33, respectively, consistent with totally uncorrelated free rotors. However, when the distribution of these quantities are calculated for nearest neighbor pairs only, we find the most probable value of $\langle (\hat{n}_i \cdot \hat{n}_j)^2 \rangle$ is 0.308 ± 0.006, which indicates the presence of local, short-ranged orientational correlations. This feature is a reflection of the fact that the probability distribution for $\hat{n}_i \cdot \hat{n}_j$, for nearest neighbors (i,j), is not constant but is well defined by the equation

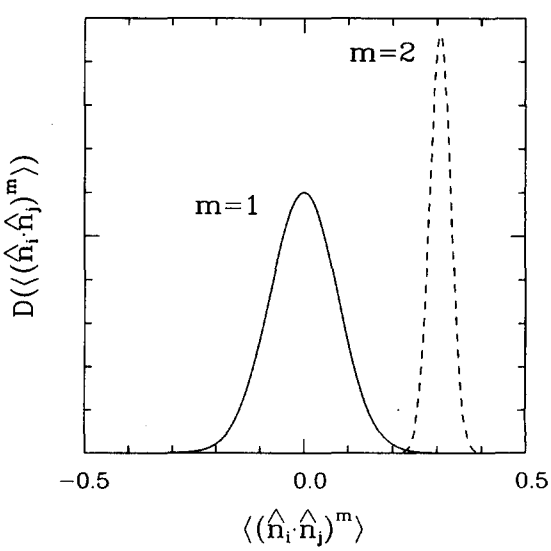

FIG. 5. The solid line shows the calculated distribution of $\langle \hat{n}_i \cdot \hat{n}_j \rangle$ over all pairs of molecules and the dashed line gives the distribution of $\langle (\hat{n}_i \cdot \hat{n}_j)^2 \rangle$ at $T = 55$ K and $P = 0.4$ GPa. The averages were taken over 10 000 mc steps.

$$P(\hat{n}_i \cdot \hat{n}_j) = 0.5 - 0.095P_2(\cos\theta_{ij}) + 0.008P_4(\cos\theta_{ij}), \quad (3)$$

where P_2 and P_4 are Legendre polynomials, the coefficients of which are accurate to within 10%.

The histogram in Fig. 6 shows the probability distribution $P(\varphi)$, where φ is the azimuthal angle of the molecular axis with respect to the Cartesian coordinate system shown in Fig. 2. The solid line is an independent representation of $P(\varphi)$, given by Eq. (4), where the expansion coefficients are evaluated as expectation values from our Monte Carlo data, as described by Press and Hüler.[39] The z coordinate is along the crystallographic c axis. The undulations in this distribution clearly show an orientational preference for the six azimuthal angles consistant with molecules oriented toward the center of the six square faces of the hexagonal cell surrounding each molecule. It is also evident from the figure that this preference is weak and that all azimuthal angles are almost equally likely. This distribution can be well described by the function

$$P(\varphi) = \frac{1}{2\pi} - 0.0083\cos(6\varphi), \quad (4)$$

where the coefficient of the second term is accurate to within 10%. Additional terms do not improve the quality of the fit.

The histogram in Fig. 7 shows the calculated probability distribution for $\cos(\theta)$, where θ is the polar angle of the molecular axes. Two features are evident. There is a preference for the molecules to orient either along the c axis or nearly normal to it, although the distribution about $\theta = \pi/2$ is very broad. The other evident feature is that the distribution is not greatly different from a straight, horizontal line, which is characteristic of spherical symmetry. The probability distribution is accurately described by

$$P(\cos\theta) = 0.5 - 0.01P_2(\cos\theta) + 0.12P_4(\cos\theta) + 0.08P_6(\cos\theta), \quad (5)$$

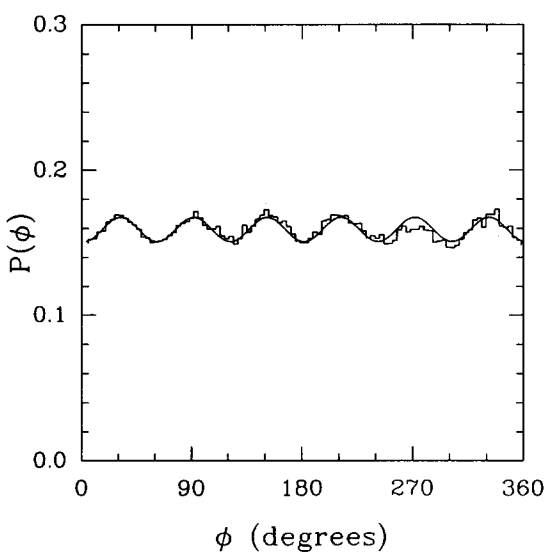

FIG. 6. The histogram is the calculated probability distribution in the azimuthal angle φ of the molecular axes versus φ, referred to the coordinate system shown in Fig. 2, in the β phase at $P = 0.4$ GPa, $T = 55$ K. The solid line is the expansion given by Eq. (4).

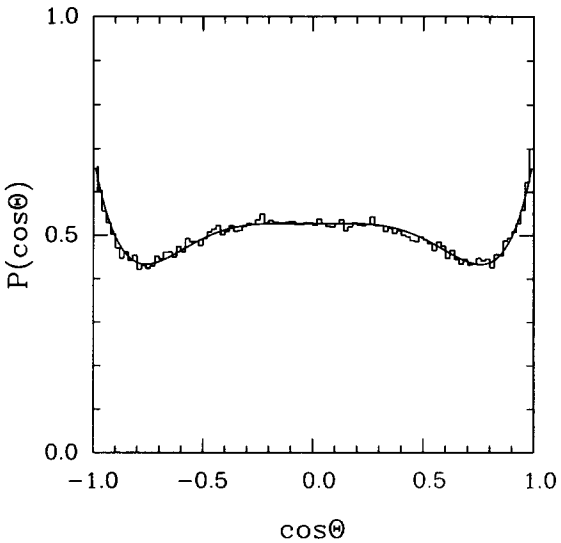

FIG. 7. The calculated probability distribution in the polar angles of the molecular axes versus $\cos\theta$ for the β phase at $P = 0.4$ GPa, $T = 55$ K. The histogram denotes the actual Monte Carlo bin averages and the solid line is the expansion given by Eq. (5).

where the coefficients of the Legendre polynomials are accurate to within 10%. The solid line represents the expansion given by Eq. (5).

The results in Fig. 7 are presented in Fig. 8 in the units used by Dunmore,[30] which is our $P(\theta)$ divided by $2\pi \sin\theta$. The dashed line represents the mean field results of Dunmore, which are qualitatively the same as van der Avoird *et al.*[31] If the broad central peak around $\pi/2$ is decomposed into two peaks, the angles $\theta \simeq 0$ and 70° are most probable. Clearly, neither $P(\theta)$ nor $P(\cos\theta)$ show any inclination for the value $\theta \simeq 56°$ that has been associated with the precession model. An examination of the instantaneous direction cosines of the molecular orientations along the Monte Carlo trajectories shows that these orientations are quite dynamic

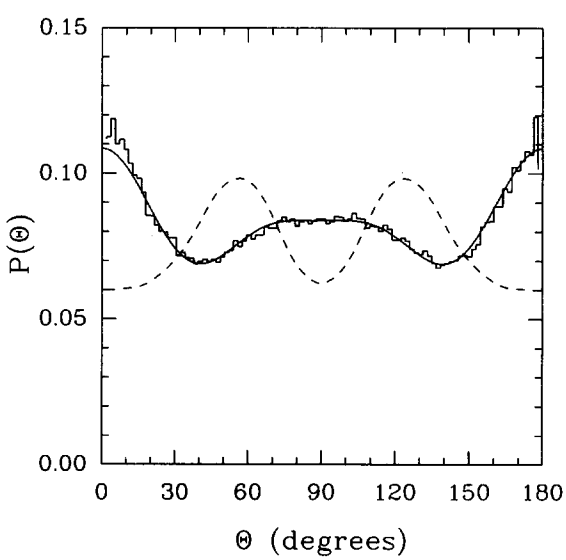

FIG. 8. The same probability and format as shown in Fig. 7 versus θ, in the units used by Dunmore (Ref. 30). The dashed line gives Dunmore's mean field results.

but not nearly what would be expected for a free rotor. Instead, these quantities tend to remain near some value for a few hundred steps along the phase space trajectories, and then abruptly change to quite different values, where they remain again for some period. This general pattern continues over the entire sequence.

It is understood that the Monte Carlo method does *not* characterize the temporal behavior of a system. Thus, the reference here and hereafter to dynamical orientational behavior is meant in the following sense. When orientations are strongly localized, the direction cosines along Monte Carlo transactions show only small fluctuations about constant, well-defined values. Conversely, simulations involving nearly free rotors have no such tendency. Instead, the direction cosines exhibit a random walk behavior over the range $-1 \leqslant u, v, w, \leqslant 1$. This is what we mean by dynamic behavior. The abovementioned case for nitrogen is intermediate between these extremes, where the number of steps spent in a localized orientation is much greater than the number of steps required to change orientations.

B. Properties along the 300 K isotherm

The solid line in Fig. 9 shows the calculated P–V curve along the 300 K isotherm and the solid symbols represent experimental data. The curve for $P \leqslant 2.5$ GPa shows our results in the fluid phase, and the inverted triangles represent the experimental data.[10] This good agreement extends to the lowest fluid pressures. Upon increasing the pressure, using a fluid-like initial configuration, stable fluid states were obtained up to $P \simeq 3.0$ GPa, above which amorphous solid behavior developed. Using a hexagonal β-N_2 initial configuration, and reducing the pressure, did not produce a stable fluid phase until $P \lesssim 2$ GPa, although slip dislocations of the hexagonal basal planes with respect to one another occurred with increasing frequency below 3 GPa. This difference in transition pressure is not surprising since similar hysteresis has been observed in other constant pressure simulations of melting.[32] Although this hysteresis limits our ability to precisely predict the melting pressure, the results are in reasonable quantitative agreement with the experimental value of melting at $P_m = 2.44$ GPa. The hysteresis does allow us to calculate both fluid and solid properties in the range $2 < P < 3$ GPa and the entropy change on melting at 2.5 GPa is $\Delta S = \Delta H / T_m = 0.62 \pm 0.02$, where H is the enthalpy, compared with an experimental value[10] of $\Delta S_{\text{exp}} = 0.66$, in units of Boltzmann's constant. The calculated volume change on melting was $\Delta V = 0.30 \pm 0.04$ cm^3/mol, compared with an experimental value[10] of $\Delta V = 0.36 \pm 0.04$ cm^3/mol. This result was determined using a 384 molecule cell. However, a cell containing 108 molecules contains more slip dislocations, where the calculated volume change upon melting is $\Delta V = 0.26 \pm 0.05$ cm^3/mol. This difference suggests that the dislocations may contribute to the melting process, and exposes a possible size dependence to these Monte Carlo results. The calculated vibron frequencies show a 1.2 ± 0.5 cm^{-1} decrease upon melting, in agreement with the experimental observations of Schiferl.[33]

At pressures $2.5 \leqslant P \leqslant 4.9$ GPa, the calculations show that the β-N_2 structure is stable along the 300 K isotherm, given a Monte Carlo cell commensurate with this structure. The squares in Fig. 9 represent the experimental P–V points[11,34] in this region and can be compared with the calculations. The c/a ratio agrees with the ideal hexagonal close packed value of 1.633, to within the statistical uncertainty, which is approximately 0.6%. This is again consistent with experiment.

The solid line in Fig. 10 at pressures $2.5 \leqslant P \leqslant 4.9$ GPa

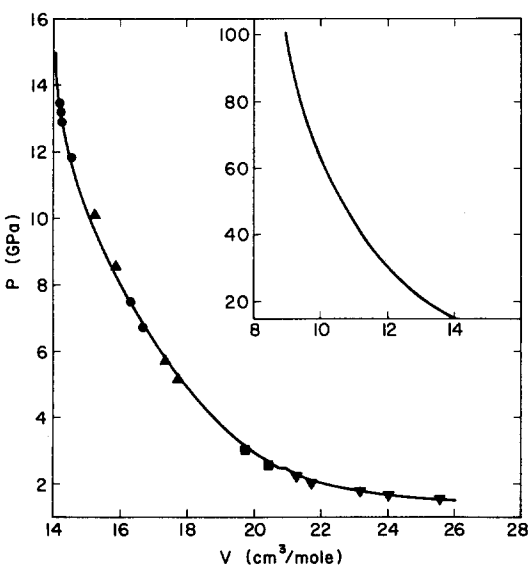

FIG. 9. The solid line in the figure and the insert gives the calculated P–V relation along the 300 K isotherm. The inverted triangles (Ref. 10) are measurements in the fluid phase, the squares (Refs. 11 and 34) in the β phase, and the triangles (Ref. 16) and circles (Ref. 18) in the Pm3n phase.

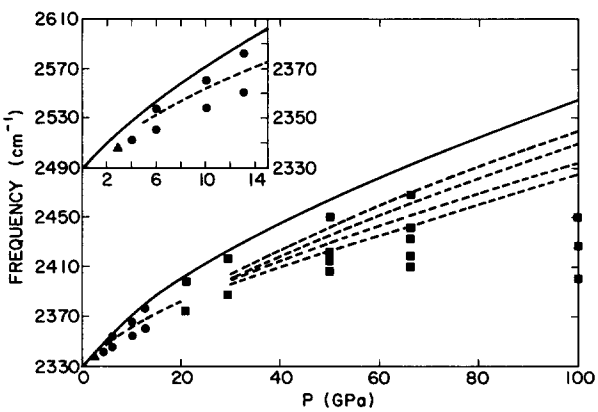

FIG. 10. The solid line for $0 \leqslant P \leqslant 2.5$ GPa gives the calculated vibron frequencies in the fluid along the 300 K isotherm and the β phase from $2.5 \leqslant P \leqslant 4.9$ GPa. The triangle (Ref. 14) and circle (Ref. 13) represent experimental data in this latter phase. From $4.9 \leqslant P \leqslant 20$ GPa, the solid and dashed line represent the calculated vibron frequencies in the Pm3n phase for the spherical and disk site molecules, respectively. The circles (Ref. 13) give the experimental results. For $P > 20$ GPa, the solid line gives the calculated vibron frequencies in the tetragonal phase associated with sites identified as spherical in the Pm3n phase, and the dashed lines give the results for the disk site molecules. The solid squares represent the experimental results (Ref. 17). The frequency scale for the insert is to the right.

shows the calculated vibron frequencies in the β phase, and the solid circle[13] and triangle[14] represents the two experimentally measured values. The nature of the orientational disorder at $(T,P) = (300\,\text{K}, 3.5\,\text{GPa})$ is noticeably different than that calculated for the same phase at $(T,P) = (55\,\text{K}, 0.4\,\text{GPa})$. The probabillty distributions $P(\varphi)$ and $P(\cos\theta)$ are nearly constant and show no clear evidence of the structure evident at the lower temperature and pressure. Moreover, $\langle \hat{n}_i \cdot \hat{n}_j \rangle = 0$ and $\langle (\hat{n}_i \cdot \hat{n}_j)^2 \rangle = 0.33$, for all molecular pairs (i,j). The probability distributions for these latter quantities are highly peaked about their average values. This is the signature of a spherically symmetric orientational distribution with no orientational correlation between neighbors. The disorder is clearly dynamic rather than static, as can be seen by following the molecular orientations along the Monte Carlo trajectories, which appear much like the signature of free rotors.

At pressures $5 \leqslant P \leqslant 20$ GPa, the cubic Pm3n phase is stable along the 300 K isotherm. The calculated P–V curve in this region is also shown in Fig. 9, and the circles[18] represent experimental results. To investigate the β-Pm3n transition, we used deformable boundary conditions with a special hexagonal representation of the cubic Pm3n structure, identical to that used by Mills *et al.*[18] in analyzing their x-ray data. A simulation with a 192 molecule cell at room temperature and 7 GPa gave results identical to our cubic representation. Upon lowering the pressure in increments of 0.5 GPa, no transition away from Pm3n symmetry was found prior to melting at approximately 2.0 GPa. It is clear that this transition involves more than a simple rearrangement of molecules and a deformation of the cell. However, in the vicinity of and on both sides of the observed transition at $P = 4.9$ GPa, either phase could be stabilized by choosing the appropriate starting configuration and boundary conditions. Thus, we obtained a volume change on transition of $\Delta V = 0.08 \pm 0.02$ cm^3/mol, at the measured transition pressure of 4.9 GPa. This is somewhat less than the measured change[12] of $\Delta V = 0.20$ cm^3/mol.

The structure of the Pm3n phase is shown in Fig. 2, where the corner and body-centered sites are represented by spheres and the two molecules on each face are represented by disks that project from the face. The spherical polar coordinates specifying the orientations of the molecules (θ,φ) are referred to the coordinate system shown in Fig. 2. At $(P,T) = (7\,\text{GPa}, 300\,\text{K})$, the calculated probability distributions $P(\varphi)$ and $P(\cos\theta)$ versus φ and $\cos\theta$, respectively, are constant for the "spherical site" molecules to within statistical uncertainty. This is consistent with a spherically symmetric orientational distribution. Moreover, the molecular orientations along the Monte Carlo trajectories fluctuate over all orientations in an apparently random fashion, reminiscent of free rotation. The probability distribution $P(\varphi)$ versus φ for disk molecules with mass centers in the bc plane is nearly constant, but there are weak peaks for orientations in the bc plane and perpendicular to it. For these same molecules $P(\cos\theta)$ forms a broad symmetric, sinusoidal peak around $\cos\theta = 0$. These distributions are shown in Fig. 11 and are consistent with a model in which the molecules uniformly sample all orientations in the disk plane and

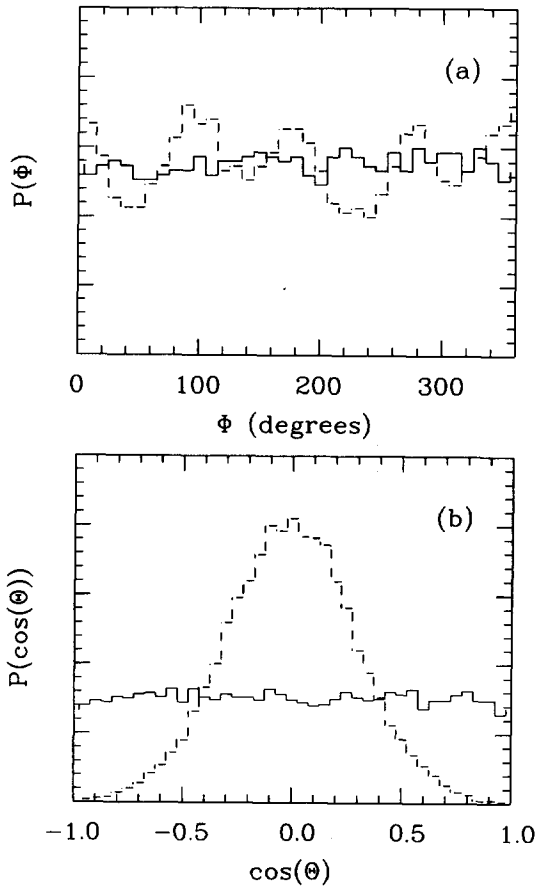

FIG. 11. The probability distribution of the molecular orientations in the Pm3n phase at $T,P = 300$ K, 7 GPa, referred to the coordinate system in Fig. 2. The solid and dashed lines on (a) give the distribution in the azimuthal angle φ for the spherical sites and the disk sites in the bc plane, respectively. The distribution in the polar angle θ is shown on (b) with the same format.

up to approximately 20° out of plane. This angle is deduced from the half-width of the peak in $P(\cos\theta)$.

The distribution $D(\langle (\hat{n}_i \cdot \hat{n}_j)^2 \rangle)$ for the Pm3n phase at 7 GPa and 300 K is shown in Fig. 12, where the $\hat{n}_i \cdot \hat{n}_j$ is the cosine of the angle between molecular axes of molecules (i,j). The distribution is taken over all pairs. It is clear that the distribution in $\langle (\hat{n}_i \cdot \hat{n}_j)^2 \rangle$ is peaked about 0.29, 0.33, and 0.44. The distribution in $\langle \hat{n}_i \cdot \hat{n}_j \rangle$ is strongly peaked around zero. To understand these results it must be recognized that there are four distinct types of pairs making up the distributions. They are sphere–sphere, sphere–disk, coplanar disk–disk, and noncoplanar disk–disk pairs of sites. Using the model mentioned above, where it is argued that the spherical site molecules sample a uniform orientational distribution and the disk site molecules have a uniform distribution for all orientations in the disk plane and at angles up to δ out of plane, it is straightforward to analytically calculate $\langle \hat{n}_i \cdot \hat{n}_j \rangle$ and $\langle (\hat{n}_i \cdot \hat{n}_j)^2 \rangle$. The model will be described in detail in a future publication. For all uncorrelated spherical–spherical site pairs these quantities give zero and 0.33, respectively. For pairs involving disk sites, these averages depend on δ. For $\delta = 25°$ we find $\langle \hat{n}_i \cdot \hat{n}_j \rangle = 0$ for all such pairs and $\langle (\hat{n}_i \cdot \hat{n}_j)^2 \rangle = 0.29$, 0.33, and 0.44, in excellent agreement

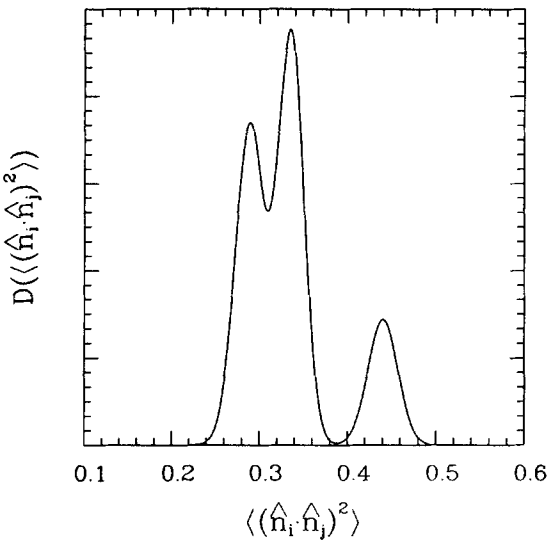

FIG. 12. The distribution of $\langle(\hat{n}_i\cdot\hat{n}_j)^2\rangle$ over all pairs of molecules for the Pm3n phase at $T,P = 300$ K, 7 GPa. The averages were taken over 10 000 mc steps.

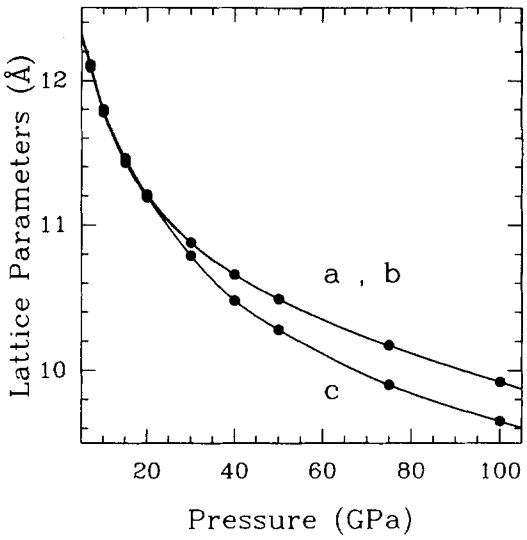

FIG. 13. The calculated a,b,c lattice parameters for a 64 molecule unit cell versus pressure, along the 300 K isotherm. The lower curve gives the c parameter and the upper a,b. Lengths are in Angstroms and the statistical error is smaller than the symbol size.

with our Monte Carlo results. This value of δ agrees quantitatively with that estimated form the half-width of $P(\cos\theta)$ for the disk molecule, shown in Fig. 11. These results and the profile of the molecular orientations along the Monte Carlo trajectories are consistent with nearly free rotation within the envelopes described above for the spherical and disk site molecules. However, the only certain conclusion is that the orientational disorder is highly dynamic in the Monte Carlo sense.

By calculating the force constants for each molecule in the Monte Carlo cell, we are able to separately identify the vibron frequencies associated with the disk and spherical sites. We find two distinct frequencies for $4.9 \leqslant P \leqslant 20$ GPa. The solid and dashed curves in Fig. 10 show these results for the spherical and disk sites, respectively. The circles[13] represent experimental data.

At pressures $P \gtrsim 20$ GPa, calculations show that a phase transition occurs from the cubic Pm3n phase into a tetragonal phase with 32 molecules per primitive unit cell, although a 64 molecule cell compatible with the primitive cell was used in most of the calculations. The lattice parameters for this cell are shown in Fig. 13 versus pressure, from which it is evident that the tetragonal transition begins at $P \simeq 20$ GPa. Calculations show that the "disk" site vibron mode frequency splits into two branches at about the same pressure, and further splits into four branches at $P \gtrsim 30$ GPa, as shown in Fig. 10. This plus the fact that both the cubic and tetragonal phases appear during simulation runs in this interval lead to the conclusion that the cubic to tetragonal transition occurs gradually over the interval $20 \lesssim P \lesssim 30$ GPa. Our results are not sufficient to comment on the order of this transition. The new structure is a minor variant of the cubic Pm3n phase, where the orientational disorder evident at lower pressures freezes out. This feature was confirmed by examining the orientations and their correlations in the same manner as was done for the β and Pm3n phases described earlier. The orientational structure is quite complicated, but several features emerge. The molecules that were on the spherical sites of the Pm3n structure now orient along the body diagonals, but no clear pattern is evident as to which diagonal is favored. The orientations of the disk molecules in chains along the **c** axis of the tetragonal cell [see Fig. 2] alternate in orientation either parallel or perpendicular to the a–c face. Adjacent molecules in neighboring chains along the **c** axis are perpendicular to one another. Chains along the **a** and **b** axes do not show such regularity, although there tends to be a propensity for neighbors to pair off two by two. Thus there are relatively large peaks in $D\langle(\hat{n}_i\cdot\hat{n}_j)\rangle$ at $\langle\cos\theta_{ij}\rangle = 0, \pi/2$. In an attempt to confirm the 32 molecule tetragonal unit cell, a 512 molecule Monte Carlo cell was examined. The resulting cell, while being tetragonal, did not exactly replicate the orientational structure of the 64 molecule cell. This implies that either the smaller cell is not a unit cell, or orientational metastability has been achieved. The calculated vibron frequencies in the tetragonal phase are qualitatively much like those measured, except that the lowest calculated mode does not decrease in frequency at high pressure, as is observed. The squares give a typical selection of experimental results[17] for the various modes in order of descending frequency.

C. Properties along the 7 GPa isobar

The solid circles in Fig. 14 show the calculated molar volumes versus temperature along the 7 GPa isobar, and the solid lines are fits through these points. At temperature $200 < T \lesssim 600$ K, the system relaxes into the cubic Pm3n structure, described in Sec. III B. The solid square gives the only experimental point[18] along this isobar, which is a linear interpolation between two pressure points very close to 7 GPa. The very nearly spherically symmetric orientational behavior of the corner and body-centered molecules, and the equal probability for all orientations in disk planes of the face

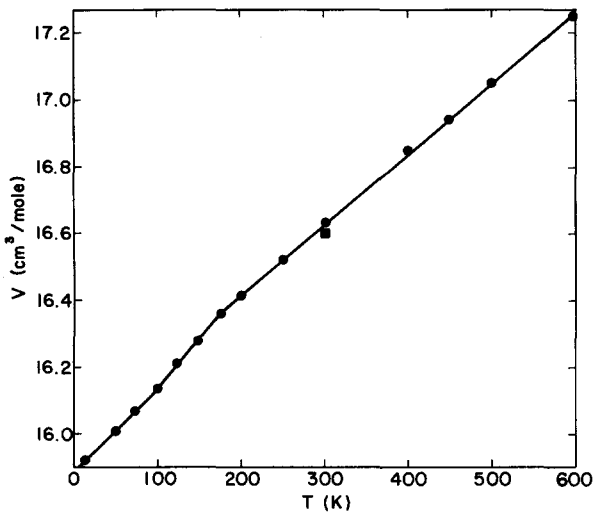

FIG. 14. The solid circles give the calculated molar volumes versus temperature along the 7 GPa isobar. The solid line is an aid through those points, and the square gives experimental data (Ref. 18).

centered molecules, that was discussed in Sec. III B at 300 K, persists at all higher temperatures up to melting. As the temperature is lowered to approximately 200 K, a degree of orientational localization occurs. By this we mean that the molecular orientations are localized for a few hundred to 10^3 Monte Carlo steps and then spontaneously jump to another orientation, and so on. The degree of localization for the disk sites is greater than for the spherical sites and, on average, the Pm3n symmetry is still preserved. This feature is reflected in Fig. 14, where the thermal expansion $\Delta V/\Delta T$ clearly changes from a constant value of 0.21×10^{-2} cm^3/mol K at higher temperatures to 0.30×10^{-2} cm^3/mol K below 200 K. As the temperature is decreased below this value, the calculated orientational localization increases. Localization of all molecules appears complete at $T\simeq120$ K, at which point a structural transition occurs from cubic to a tetragonal phase that persists to zero Kelvin. This transition is not only evidenced by a change in $\Delta V/\Delta T$ to about 0.25×10^{-2} cm^3/mol K below 120 K, as shown in Fig. 14, but also by the splitting of the **a,b** lattice parameters from **c**. This is shown in Fig. 15, where the solid squares are the calculated points and the solid lines are fits through those points. Above $T\simeq120$ K the single line shows that all three lattice parameters are of the same length and, below that temperature, the **a,b** lattice parameters follow the upper curve and **c** the lower. At all temperatures the angle between these lattice vectors is $\pi/2$. This loss of symmetry at low temperatures is definitely due to orientational ordering over the range $120\lesssim T\lesssim200$ K. It is clear that this structure is very similar to the orientationally ordered, tetragonal phase found at higher pressures along the 300 K isotherm. Numerous other metastable structures were found at low temperature and, although quite similar to the quadrupole favored tetragonal phase, they were found to have higher Gibbs free energy in the limit of zero temperature.

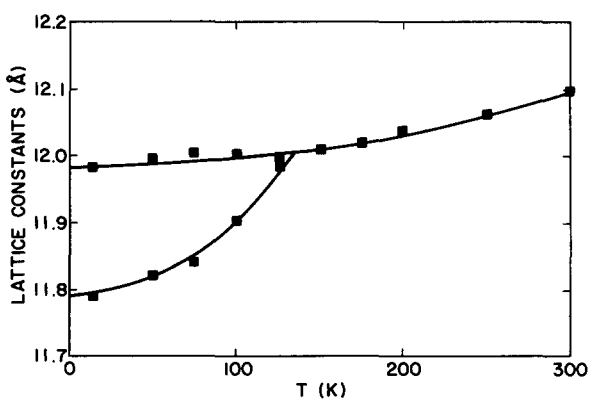

FIG. 15. Calculated lattice parameters for a 64 molecule unit cell versus temperature along the 7 GPa isobar. The lower curve gives the c parameter and the upper a,b. The solid line is an aid through the calculated points.

The calculated vibron frequencies versus temperature at 7 GPa are shown in Fig. 16, where the circles are calculated using a hexagonal 192 molecule Monte Carlo cell, the squares for a 64 molecule cell, and the triangles for a 32 molecule cell. There are several observations. The high frequency branch is associated with the spherical site molecules identified in the Pm3n phase. It is initially independent of temperature but then decreases until melting, where it seems to merge with the low frequency solid and fluid branches. The low frequency branch is associated with the disk sites on the faces and is relatively more constant with temperature. It seems to merge into the fluid branch vibron at melting, which occurs at $T_m\simeq650$ K in this calculation. The results are qualitatively very similar to the experiment[35] also shown

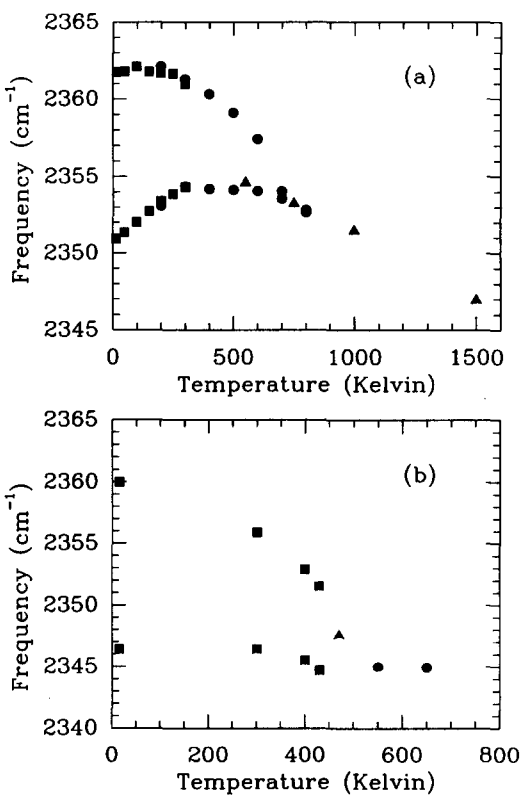

FIG. 16. (a) The calculated vibron frequencies (cm^{-1}) versus temperature along the 7 GPa isobar. The triangles, squares, and circles are determined using 32, 64, and 192 molecule Monte Carlo cells, respectively. The statistical error in the calculated values is about $\pm$ 1 cm^{-1}. (b) The experimental data.

in Fig. 16, with two small but possibly important exceptions. The linear increase of about 4 cm^{-1} in the lower mode frequency with temperature in the range $0 \leqslant T \lesssim 200$ K is contrary to experiment, which shows this mode to be temperature independent. Second, there is some indication that the lower branch splits in the tetragonal phase, much like it does in the high pressure tetragonal phase at room temperature. However, the indication of splitting is only on the order of the uncertainty in our frequency calculations, $\Delta\nu \approx \pm 1.0$ cm^{-1}, and may not be experimentally resolvable.

IV. DISCUSSION AND CONCLUSIONS

The calculated thermodynamic properties, structures, and vibron frequencies in solid N_2 generally show remarkably good agreement with experiment over a wide range of pressures and temperatures, in several different phases. At $P = 0$, the calculated structure stabilized into the observed hexagonal β phase over the experimentally observed range[2-5] $35.6 \leqslant T \leqslant 63.1$ K, although melting did not occur until $T \simeq 76$ K. The calculated temperature dependence of the molar volume and the thermal expansion coefficient[28,29] agree quite well with experiment, as shown in Figs. 3 and 4. An additional point calculated at $(P,T) = (0.4\ \text{GPa}, 55\ \text{K})$, gave a molar volume within 2.5% of its measured value.[7] Calculations along the 300 K isotherm also produced a stable β-N_2 phase over the region it is experimentally observed,[10-12] $2.5 \lesssim P \lesssim 4.9$ GPa. Although there are only two measured values[11,34] of (P,V) in this region, Fig. 9 shows that they and the calculations agree quite well. Over the entire (T,P) field of the β phase, the calculated c/a ratio is equal to its ideal value, within a statistical uncertainty of 0.6%. The calculated vibron frequencies, shown in Fig. 10, are about 6 cm^{-1} higher than the only two measured values[13,14] at 2.8 and 4.1 GPa.

Although we were unable to determine the β-Pm3n transition pressure along the 300 K isotherm, due to the aforementioned incompatibility of the Monte Carlo cell with the unit cells for both phases, the cubic Pm3n phase did form a stable structure in the region $4.9 \leqslant P \lesssim 20$ GPa. As shown in Fig. 9, the calculated P–V relation in this region is in excellent agreement with experiment.[16,18] The calculated vibron frequencies in Fig. 10 show two branches which is a characteristic signature of the Pm3n phase. The upper branch is identified with the spherical site molecules and the lower with the disk sites. The quantitative agreement with experiment[13,17] is good, though the calculated frequencies are consistently a bit too high. It is not clear whether this is due to our potential model or the nature of our calculation. An interesting feature of the calculations is that the β-phase vibron frequencies seem to merge continuously across the transition with the spherical site frequencies of the Pm3n phase. To understand this we examined a spherical harmonic expansion of the pair distribution function for both phases close to the transition boundary. The leading term, which is spherically symmetric and depends only on the mass center separations, and the two leading orientationally dependent terms in both phases agree very closely for intermolecular separations out to and somewhat beyond nearest neighbor separations. This means that the crystal field experienced by each molecule in both phases, which is responsible for the shift of the vibron frequencies from their gas phase values, is nearly the same and thus accounts for the observed result.

Above 20 GPa, the calculations show that a phase transformation occurs into a tetragonal phase with 32 molecules per unit cell which is a minor variant of the Pm3n structure. This is confirmed by the lattice parameters shown in Fig. 13, where the lattice vector **c** departs from **a** and **b** just above 20 GPa. The transition is complete by 30 GPa and orientational analysis confirms that the dynamic orientational disorder of the Pm3n phase freezes out and lowers the symmetry. The calculated vibrons in this phase show that the upper branch, associated with the spherical site molecules, is undisturbed by the transition but the mode associated with the disk sites splits into four distinct branches. This is remarkably like the experimental observations,[17] except that the quantitative comparison gets increasingly worse at higher pressures. This discrepancy is interesting because of the ongoing controversy about the observed softening of the vibron frequencies at high pressures. Our calculational method should be accurate at these high pressures, although it does not account for factor group splitting, which can be interpreted as responsible for the lack of mode softening observed in recent infrared studies and other measurements on isotopic mixtures of hydrogen,[36] whereas Raman studies[37] on pure H_2 or D_2 clearly show this effect. The same interpretation could be applied to N_2, although our calculations give splittings qualitatively similar to experiment as a consequence of different site symmetries of the disk molecules, and not from factor group splitting. Another interpretation of our quantitative failure may be an inaccurate representation of the potential at high pressures, due to charge rearrangement. The situation is not resolved.

Along the isobar at 7 GPa our calculations show the Pm3n phase is stable from $200 \lesssim T \lesssim 600$ K. The solid melts at this upper limit, which is substantially above the observed temperature of melting, $T_m = 484$ K. As shown in Fig. 14, the thermal expansion is constant over the entire temperature range of this phase, and the volume at 300 K agrees well with experiment.[18] As the temperature is decreased, the orientational disorder becomes increasingly hindered until, at $T \simeq 200$ K, the molecules begin to orientationally localize along well-defined lattice directions. However, the structure remains cubic until $T \lesssim 120$ K, whereupon it transforms into a tetragonal phase, which persists to zero Kelvin. This transition is clearly identified by a change in the lattice parameters, shown in Fig. 15. Accompanying this transition is an orientational ordering of the molecules. There are a number of interesting features. First, the tetragonal phase is very similar to that found at room temperature above 30 GPa. Second, it is also very similar to a structure predicted at low temperature in a previous molecular dynamics simulation.[21,38] Unfortunately, this structure is slightly different from the $R\bar{3}c$ lattice inferred from x-ray diffraction measurements,[18] though the differences are not great. Nevertheless, the calculated structural transition temperature is very close to the experimentally deduced value[18] of approximately 140 K. The relative stability of these two structures appears to be

very sensitive to the orientational character of the intermolecular potential, including the electrostatic terms. For example, the neglect of these latter terms results in the stability of R3c.

A number of calculations were made at high pressures and low temperatures, comparing the tetragonal structure to the $R\bar{3}c$ and R3c phases. Using the $R\bar{3}c$ initial configuration at 7 GPa and 15 K, the system relaxed to a metastable R3c structure, which transformed to the tetragonal phase upon increasing the temperature to 75 K. By comparing enthalpies of R3c and the tetragonal phases along the 15 K isotherm, it was found that the tetragonal structure becomes unstable above 60 GPa.

The orientational disorder in β-N_2 was not unambiguously resolved in early x-ray diffraction studies,[6] and two models that equally well satisfied the data emerged. The favored model was one in which the molecules execute nearly free precession about the c axis at an angle $\theta \simeq 56°$. In the other model the molecules maintain approximately the same polar angle but are static and randomly oriented along the sixfold degenerate orientations defined by the $P6_3/mmc$ crystal symmetry, that can be delineated by six values of the azimuthal angle φ. Supporting these models is that at this angle θ, each molecule either points toward a square, open face of the cage formed from the nearest neighbors or, in the precession model, pass very near the centers of all the square faces. These situations are favorable from steric considerations. Another model that is equally satisfactory is one in which the molecules undergo nearly free rotation or randomly hop from one of the six degenerate orientations to another over a time span short compared to the experimental period of measurement.

It has been observed that x-ray diffraction, neutron scattering, and the NQR measurements[6–9] all conclude that $\langle Y_{20}(\cos\theta)\rangle \simeq 0$. Several theoretical calculations[30,31] have also arrived at this same conclusion, but interpret it differently. Unfortunately, the accumulated information is not sufficient to clearly distinguish between the above mentioned models, which are all expected to give very small averages for Y_{20}. As pointed out by Press and Hüller,[39] distinguishing between the free rotor and precession models is particularly troublesome since the value of θ for which the function $Y_{20} = 0$, is very near the predicted precession angle.

Our calculated results at $P,T = (0.4\ \text{GPa}, 55\ \text{K})$, which coincides with neutron diffraction studies,[7] shows the following features. The distributions in the averages $\langle \hat{n}_i \cdot \hat{n}_j \rangle$ and $\langle (\hat{n}_i \cdot \hat{n}_j)^2 \rangle$, taken over all pairs, shows sharp peaks at 0.0 and 0.33, respectively. These are shown in Fig. 5, and are consistent with a totally random distribution of relative orientations. However, when these distributions are produced for nearest neighbor pairs only, there is a small but statistically significant shift in $\langle (\hat{n}_i \cdot \hat{n}_j)^2 \rangle$. This indicates the existence of weak, short-ranged correlations which are reflected in the fact that $P(\hat{n}_i \cdot \hat{n}_j)$ is not constant in $\cos(\theta_{ij})$. The probability distribution $P(\varphi)$, displayed in Fig. 6, shows six peaks that are located at azimuthal angles identical to the directions of the six square faces on the nearest neighbor cage. It is also notable that these peaks are small modulations on an otherwise uniform distribution. The probability distribution $P(\cos\theta)$, shown in Fig. 7 versus $\cos\theta$, shows a sharp peak around $\theta = 0$ and a broad, flat peak about $\theta = \pi/2$. This latter peak can be decomposed into two Gaussian peaks centered at $\theta \simeq 70°$ and 110°. Thus, polar orientations along the **c** axis and about 20° off the ab plane are most preferred. Similar conclusions come from $P(\theta)$ versus θ, which is in sharp contrast to the mean field distributions.[30,31] Interestingly, the distribution is near a minimum at the quoted precision angle of 56°. It is also evident that the departure in the polar angle from a uniform distribution is not great, although more so than for φ. At the experimental condition,[7] our calculated value $\langle Y_{20} \rangle = -0.004$ and, upon increasing the temperature along this 0.4 GPa isobar, it goes through zero and becomes positive at 100 K. Upon increasing the pressure at 100 K, it decreases and becomes a small negative value at 1.0 GPa. Further details will be given in a forthcoming paper. An examination of the molecules along a Monte Carlo trajectory reveals that they do not sample all orientations as would be expected for a nearly free rotor. Instead they appear to remain close to a specific orientation for quite a few steps, and then quickly move to a new orientation, and so on. It is noticed that when one molecule is oriented along the **c** axis the six nearest neighbors in the same plane are often oriented in a pinwheel arrangement, very much like the (1,1,1) plane of α-N_2. These pinwheels seem to form, disperse, and then form elsewhere, much like a propagating excitation. It must be emphasized that this is a highly speculative hypothesis, but it is consistent with our probability distributions. Below the orientational ordering transition temperature we find pinwheel arrangements, much like Mandell[40] found in his simulation of point quadrupoles on a rigid hcp lattice.

To summarize our findings, the results show that the molecules are not precessing, even though the average polar angle $\langle \theta \rangle$ and $\langle Y_{20} \rangle$ are very close to that specified by that model. Nor is the static, randomly disordered model or the weakly modulated free rotor picture satisfactory. Instead, the behavior seems to be intermediate between these latter two cases, where frequent hopping occurs in such a way that all orientations are nearly uniformly sampled.

Another point studied extensively in the β phase was at $(T,P) = (300\ \text{K}, 3.5\ \text{GPa})$. Unlike the lower temperature point described above, there is no clear evidence of a sixfold modulation in $P(\varphi)$ and $P(\cos\theta)$ is nearly constant for all values of $\cos\theta$. Also $\langle (\hat{n}_i \cdot \hat{n}_j) \rangle$ and $\langle (\hat{n}_i \cdot \hat{n}_j)^2 \rangle$ equal zero and 0.33, respectively. This implies that the orientational sampling is much more uniform than we found at low temperature and that there is little or no correlation in the angular motion between neighboring molecules. An examination of the Monte Carlo trajectories show dynamic behavior that is much more free rotor-like than at (0.4 GPa, 55 K), but we are still reluctant to rule out the possibility of rapid, uncorrelated deployment between orientationally equivalent sites. A picture of β-N_2 emerges. At low temperatures and pressures, near the α–β phase boundary, the orientational motion is quite hindered and the modulation described in connection with the (0.4 GPa, 55 K) point is substantially more pronounced, as are the orientational correlations. At high tem-

peratures, near melting, the orientational distribution is isotropic and the orientational motion is highly dynamic. This is in contrast to some previous experimental interpretations.[33] Increasing pressure along an isotherm acts to hinder the motion, as expected. Clearly, the orientational character of β-N_2 changes considerably over its field of stability.

Experimental evidence[12-16] for orientational disorder in the cubic Pm3n phase comes mostly from x-ray diffraction measurements, where the results were argued to be consistent with a spherically symmetric disorder for the corner and body-centered molecules and a uniform planar distribution for the molecules on the faces. It could not be established if the molecules act as free rotors, with the face molecules constrained only to a plane, or if the molecules reorient randomly along the various degenerate orientations.

The results of our calculations in the Pm3n phase at $(T,P) = (300\ \text{K}, 7\ \text{GPa})$ show $P(\cos\theta)$ and $P(\varphi)$ to be constant for spherical site molecules, indicative of a uniform orientational distribution over a unit sphere. For the disk site molecules in the bc plane, $P(\varphi)$ is nearly constant with weak peaks favoring orientations either in the bc plane or normal to it. As shown in Fig. 11, $P(\cos\theta)$ has a large, broad peak, with about a 20° half width, centered about $\cos\theta = 0$. These results are clearly consistent with the molecules almost uniformly sampling all orientations in and within about 20° of the plane of the disk. The conclusions are identical for disk site molecules on all planes.

Most revealing is the analysis of the distributions $D(\langle \hat{n}_i \cdot \hat{n}_j \rangle)$ and $D(\langle \hat{n}_i \cdot \hat{n}_j)^2\rangle$, the latter is shown in Fig. 12. By assuming uniform sampling in the plane and to an angle of $\delta = 25°$ out of plane, analytical calculations of $\langle \hat{n}_i \cdot \hat{n}_j \rangle$ and $\langle (\hat{n}_i \cdot \hat{n}_j)^2 \rangle$ for the different pairs of molecules exactly reproduce the peaks in these two distributions at zero, 0.29, 0.33, and 0.44. The success of this model, including the fact that δ agrees with the half width of the distribution in Fig. 11, is convincing evidence that the disk molecules do uniformly sample the envelope described above, as suggested by experimental interpretations. It is also evident that if any orientational correlations between molecules exist, they are extremely weak. Thus, the spherical site molecules clearly sample a uniform, spherical distribution, and there is no evidence of orientation correlations between neighbors. The disk site molecules sample all orientations nearly uniformly within the envelope of a planar disk. There is a weak modulation showing a preference for the molecules to orient either in plane or normal to it. There are no noticeable orientational correlations between disk site molecules or with the spherical site molecules. The orientational behavior along a Monte Carlo sequence at 300 K is certainly suggestive of weakly modulated free rotation, whereas at 200 K and below, the trajectories show sporadic hopping between localized orientational sites.

It is not the purpose of this paper to dwell on the melting results since they are truly complicated and require much more attention than was given here. However, these studies did reveal some interesting features. A reduction in pressure along the 300 K isotherm, using the solid β-N_2 starting configuration, did not show melting until $P \lesssim 2$ GPa, about 0.5 GPa below the experimentally observed transition.[10,11] However, calculations did reveal planar slip dislocation occurring with increasing frequency as the pressure was lowered below 3 GPa. Increasing pressure from below the transition, using a fluid-like starting configuration did not reveal a solid structure until $P \gtrsim 3.0$ GPa. There is calculational hysteresis. Nevertheless, by any measure the predicted transition pressure is not far from the observed one of 2.44 GPa. The calculated volume change on melting is $\Delta V = 0.30 \pm 0.04$ with a 384 molecule cell, compared with 0.36 ± 0.04 experimentally.[10] This, in addition to the calculated vibron shift of $-1.2 \pm 0.5\ \text{cm}^{-1}$ upon melting, which is also in good agreement with experiment,[33] is gratifying. Additional work is presently being done on melting.

The numerous phases investigated in this work and the transitions between them expose some calculational features that need to be discussed. The use of an (N,P,T) ensemble with deformable boundary conditions is clearly a major advance in predicting the nature of phase transitions. Not only does it provide for volume fluctuations, which are an important part of many transitions, but also the deformable boundary conditions may accommodate the spontaneous change in symmetry between the phases involved in a transition. In these cases, no *a priori* judgement about the nature of the structures need be imposed. Unfortunately, for any given number of particles in the Monte Carlo cell it is sometimes not possible to deform even a general triclinic cell so that it is an integral multiple of the unit cell of both phases. Thus, the utility of the abovementioned technique is diminished. There are also situations in which various metastable states exist, separated by a large potential barrier as, for example, in solid CO_2.[41] It is then often the case that any optimization or simulational procedure will not evolve to the true thermodynamic ground state, determined by the minimum Gibbs free energy, in an acceptably small amount of time. Another difficulty has to do with the fact that we usually deal with ideal systems, without free surfaces, vacancies, impurities, dislocations, grain boundaries, or other disruptions to perfect symmetry. These features can be influential in the behavior of real transitions, as is particularly thought to be the case in melting.[42] We use various techniques which resolve or at least ameliorate these difficulties, but, in the final analysis, there are always uncertainties in the prediction of phase transitions and that must be recognized here.

ACKNOWLEDGMENTS

We wish to thank the CSU University Computer Center for providing time on the CDC Cyber 205 computer, within the CSU Supercomputing project. J. B. would like to acknowledge Mark Robbins for many useful and stimulating discussions. This work was supported by the U.S. Department of Energy (DOE) Grant No. DE-FG02-86ER45238.

[1] L. Vegard, Z. Phys. **58**, 497 (1929); M. Ruhemann, *ibid.* **76**, 368 (1932); L. H. Bolz, M. E. Boyd, F. A. Mauer, and H. S. Peiser, Acta Crystallogr. **12**, 247 (1959).
[2] A. F. Schuch and R. L. Mills, J. Chem. Phys. **52**, 6000 (1970).
[3] E. M. Horl and L. Marton, Acta Crystallogr. **14**, 11 (1961); J. A. Venables, Philos. Mag. **21**, 147 (1970); J. A. Venables and C. A. English, Acta Crystallogr. Sect. B **30**, 929 (1974).

[4]W. E. Streib, T. H. Jordan, and W. Lipscomb, J. Chem. Phys. **37**, 756 (1962).
[5]W. M. Cheng, W. B. Daniels, and R. K. Crawford, Phys. Rev. B **11**, 3972 (1975).
[6]W. E. Streib, T. H. Jordan, and W. N. Lipscomb, J. Chem. Phys. **37**, 2962 (1962); T. H. Jordan, H. W. Smith, W. E. Streib, and W. M. Lipscomb, *ibid.* **41**, 756 (1964).
[7]B. M. Powell, C. Dolling, and H. F. Nieman, J. Chem. Phys. **79**, 982 (1983); B. M. Powell, H. F. Nieman, and G. Dolling, Chem. Phys. Lett. **75**, 148 (1980).
[8]F. W. Terman and T. A. Scott, Bull. Am. Phys. Soc. **3**, 23 (1958); A. S. DeReggi, P. C. Canepa, and T. A. Scott, J. Magn. Reson. **1**, 144 (1969).
[9]M. A. Doverspike and M. S. Conradi, Phys. Rev. B **30**, 4905 (1984).
[10]R. L. Mills, D. H. Liebenberg, and J. C. Bronson, J. Chem. Phys. **63**, 1198, 4026 (1975).
[11]D. Schiferl, D. Cromer, and R. L. Mills, High Temp. High Pressures **10**, 493 (1978).
[12]D. Cromer, R. L. Mills, D. Schiferl, and L. Schwalbe, Acta Crystallogr. B **37**, 8 (1981).
[13]R. LeSar, S. Ekberg, L. Jones, R. L. Mills, L. A. Schwalbe, and D. Schiferl, Solid State Commun. **32**, 131 (1979).
[14]S. Buchsbaum, R. L. Mills, and D. Schiferl, J. Phys. Chem. **88**, 2522 (1984).
[15]D. Schiferl, S. Buchsbaum, and R. L. Mills, J. Phys. Chem. **89**, 2324 (1985).
[16]B. Olinger, J. Chem. Phys. **80**, 1309 (1984).
[17]R. Reichlin, D. Schiferl, S. Martin, C. Vanderborgh, and R. L. Mills, Phys. Rev. Lett. **55**, 1464 (1985).
[18]R. L. Mills, Bart Olinger, and D. T. Cromer, J. Chem. Phys. **84**, 2837 (1986).
[19]R. LeSar, J. Chem. Phys. **81**, 5004 (1984).
[20]V. Chandrasekharam, R. D. Etters, and K. Kobashi, Phys. Rev. B **28**, 1095 (1983).
[21]S. Nosé and M. L. Klein, Phys. Rev. B **33**, 339 (1986); Phys. Rev. Lett. **50**, 1207 (1983); Mol. Phys. **50**, 1055 (1983).
[22]R. D. Etters, V. Chandrasekharan, E. Uzan, and K. Kobashi, Phys. Rev. B **33**, 8615 (1986).
[23]R. Berns and A. van der Avoird, J. Chem. Phys. **72**, 6107 (1980).
[24]R. LeSar and R. Gordon, J. Chem. Phys. **78**, 4991 (1983).
[25]P. Huxley and J. Murrell, J. Chem. Soc. Faraday Trans. **79**, 323 (1983).
[26]J. Belak, Ph.D. thesis, Colorado State University, 1988.
[27]J. Belak, R. D. Etters, and R. LeSar, J. Chem. Phys. **89**, 1625 (1988).
[28]J. R. Brookerman and T. A. Scott, J. Low Temp. Phys. **12**. 491 (1973).
[29]I. N. Krupskii, A. I. Prokhvatilov, and A. I. Erenburg, Sov. J. Low Temp. Phys. **7**, 178 (1975); [Fiz. Nizkikh Temp. **1**, 359 (1975)].
[30]P. V. Dunmore, J. Low Temp. Phys. **24**, 397 (1976).
[31]A. van der Avoird, W. Briels, and A. Jansen, J. Chem. Phys. **81**, 3658 (1984).
[32]S. Nosé and F. Yonezawa, J. Chem. Phys. **84**, 1803 (1986); D. K. Chocappa and P. Clancy, Mol. Phys. **61**, 597 (1987).
[33]D. Schiferl (unpublished results).
[34]D. Schiferl, D. Cromer, R. Ryan, A. Larson, R. LeSar, and R. L. Mills, Acta Crystallogr. Sect. C **39**, 1151 (1983).
[35]D. Schiferl (private communication).
[36]Bill Daniels (private communication).
[37]H. K. Mao, P. M. Bell, and R. J. Hemley, Phys. Rev. Lett. **55**, 99 (1985).
[38]S. Nose and M. L. Klein, Phys. Rev. B **33**, 339 (1986).
[39]W. Press and A. Huller, J. Chem. Phys. **68**, 4465 (1978).
[40]M. J. Mandell, J. Chem. Phys. **60**, 1432, 4880 (1974).
[41]R. D. Etters and B. Kuchta, J. Chem. Phys. **90**, 4537 (1989); B. Kuchta and R. D. Etters, Phys. Rev. B **38**, 6265 (1988).
[42]D. Frenkel, Phys. Rev. Lett. **56**, 858 (1986).